



Structural Control Over Self-Assembled Crystals of π -Conjugated Poly(3,3''-didodecyl-quaterthiophene) for Organic Field-Effect Transistor Applications

Mi Jang and Hoichang Yang*

Department of Advanced Fiber Engineering, Inha University, Incheon 402-751, Korea

Liquid-crystalline (LC) poly(3,3''-didodecyl-quaterthiophene) (PQT-12) was investigated to optimize its side alkyl ordering and π -conjugated structure for high performance organic field-effect transistor (OFET) applications. Initially, low-crystal films spun-cast on OTS-treated SiO₂ substrates were further crystallized via either thermal or solvent treatments. At temperatures (125–138 °C) driving a LC state of PQT-12, mobile chains were better migrated into preformed crystals. The resulting films showed highly crystal nanofibrils, in which π -conjugated polymer backbones (with a conjugated backbone spacing, $d_{(010)}$ of 3.80 Å) and the orientation of self-assembled side-chains were tilted with respect to the film surface, respectively. However, via melting or solvent exposure providing isotropic states, film crystallization generated less ordered crystals with randomly oriented side-chains, increasing $d_{(010)}$ up to 4.16 Å. As a result, the usage of LC characteristic allowed us to consistently achieve the desirable crystal structure of PQT-12 and to robustly obtain high field-effect mobility for FET applications.

Keywords: PQT-12, Organic Electronics, Orientation, Conjugation.

1. INTRODUCTION

Organic field-effect transistors (OFETs) incorporating solution-processable, polymeric semiconductors have been widely studied due to their potential in fabricating integrated circuits for large-area and low-end electronics.^{1–7} The low-cost solution or liquid fabrication techniques, coupled with physically compact, lightweight, and flexibility, have driving force in research interest in organic electronics. Most works have been focused on optimizing and inventing device fabrication for various solution-processable semiconductors to achieve high performance in OFETs, which have produced higher hole mobilities (μ_{FETs}) up to 0.15 cm²/Vs.^{8,9}

In order to improve solubility of π -conjugated polymer semiconductors, various side-chains have been incorporated into these backbones.^{9,10} During crystallization, conjugated backbone chains are stacked by π - π interaction into one dimensional (1D) nanofibrils and are separated in the other by the alkyl side chains.¹¹ In this case, these side chains may either interfere or enhance molecular ordering of π -conjugated backbones, during direct solution-processing methods: spin-, drop-casting, screen printing,

ink-jet printing, etc.² For regioregular poly(3-alkyl thiophene)s (RR P3ATs) with the shorter side-chain (SC) interval, spacings of layered polymer backbone ($d_{(100)}$) and intermolecular π overlap ($d_{(010)}$) in these crystals tend to increase monotonically with an increase in SC length (l_{SC}). Values of $d_{(100)}$ and $d_{(010)}$ increase from 16.1 to 25.5 Å and from 3.74 to 3.90 Å, respectively, with an increase of l_{SC} from hexyl (C₆H₁₃) to dodecyl (C₁₂H₂₅) causing degradation of crystallinity and μ_{FET} .^{9,10}

Although poly(3-dodecyl thiophene) and poly(3,3''-didodecyl-quaterthiophene) (PQT-12) have the same type of SC substituent, PQT-12 shows much shorter values of $d_{(100)}$ and better π -conjugated nanostructures in cast films, especially, after thermal annealing.⁹ It seemed to be related to the molecular backbone architecture with longer SC interval (~15.5 Å), which effectively minimizes steric hindrance of the bulky SCs on the reformation of both polythiophene (PT) backbones and SCs. Among π -conjugated organic thin films, PQT-12 films with well controlled nanostructures provided a high μ_{FET} of 0.07–0.12 cm²/Vs and good on/off current ratios (>10⁵) in OFET.^{8,13,14} In particular, the relatively lower amount of the electron-donating alkyl groups could provide the larger stability against oxidative doping, when compared to RR P3ATs.⁸

*Author to whom correspondence should be addressed.

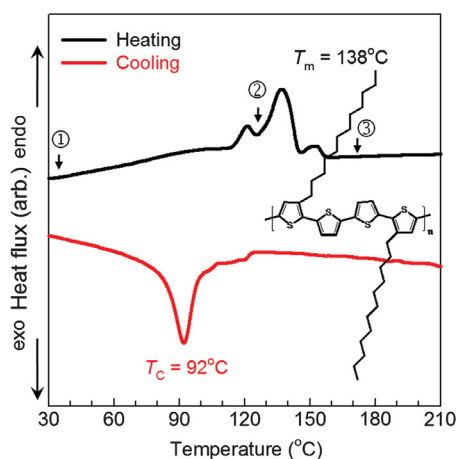


Fig. 1. DSC heating and cooling curves of PQT-12 powder. (The inset represents chemical structure of PQT-12).

Liquid crystalline (LC) characteristics of PQT-12 were indicated by differential scanning calorimetry (DSC) (see Fig. 1). At a narrow region with temperature ranging from 125 to 138 °C, typical PQT-12 might have a LC state: at

130 °C (②), self-assembled structure of PQT-12 was still maintained due to strong π - π interaction, although the interdigitated structure of SCs was dissociated. Above melting temperature (T_m) = 138 °C, e.g., 170 °C (③), the π - π interaction to hold ordered LC structure completely disappeared and PQT-12 became isotropic.¹²

In general, the presence of the long SCs on π -conjugated PT chains is considered as one of obstacles in developing highly ordered crystallites under fast solvent evaporation processes with spin-casting warm or hot solutions on relatively colder substrates, in comparison to the well ordered self-assembly of P3HT from a marginal solvent with temperature-dependent solubility.¹¹ In addition, dispersed nano-aggregates or gel-like solutions driven by strong π - π interactions of PQT-12 were easily obtained, when their solutions were stored or slowly evaporated.¹⁴⁻¹⁶ From our preliminary result, it was found that melt-crystallized or solvent-annealed PQT-12 films showed low electronic performances in OFETs, when compared to those of P3AT systems. However, crystalline growths of the mobile PQT-12 chains and the corresponding nanostructures have not been systematically

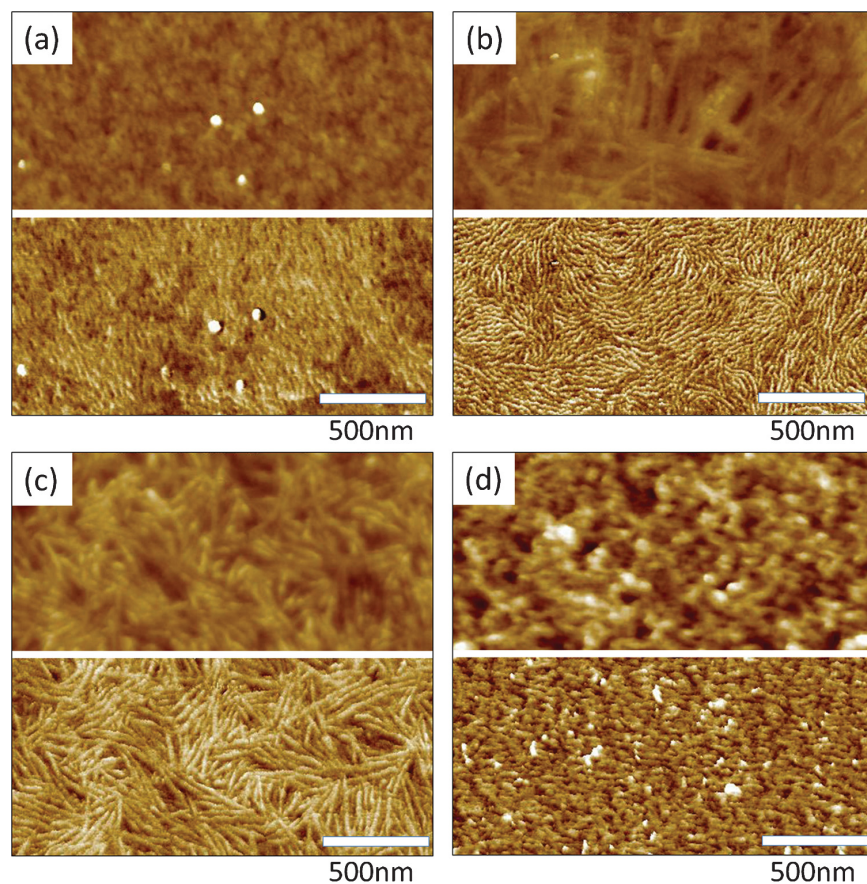


Fig. 2. AFM topographic (top) and phase (bottom) images of (a) the as-spun and subsequently post-treated (b-d) PQT-12 films on OTS-treated SiO₂/Si substrates: (b), annealed at 130 °C for 2 hr; (c) slowly crystallized from the melt (at 170 °C) with 1 °C/min; (d) solvent-annealed under TCB vapor (20 °C, 1 mm Hg).

investigated, although they often disturbed solution film fabrication for high performance OFETs.

Here, we have investigated phase behaviors of LC-type PQT-12 (number average molecular weight = 31 kDa, American Dye Source) via solution film casting and various post treatments. 50–60 nm thick PQT-12 films were spin-cast on OTS-treated SiO₂ (300 nm thick)/highly n-doped Si substrates held at 60 °C from warm trichlorobenzene (TCB, 80 °C). Based on the DSC result (Fig. 1), as-spun films were either thermally treated, especially, at the arrow-marked T_s (⊙ 130 °C and ⊙ 170 °C), or were solvent-annealed for 30 min under TCB vapor pressure (at 25 °C, 1 mm Hg). In the case of thermal treatments, each as-spun film was annealed at 130 °C for 2 hr or slowly melt-crystallized from 170 °C to 30 °C (under N₂ atmosphere: H₂O and O₂ < 0.1 ppm), respectively.

2. RESULTS AND DISCUSSION

Figure 2 represented AFM topographic and phase images of the as-spun and further post-treated PQT-12 films. As shown in Figure 2(a), the as-spun films did not show any clear crystal feature, while 130 °C annealed sample showed highly long crystal nanofibrils (length, $L > 5 \mu\text{m}$;

lateral width, $L_w = 18 \pm 2 \text{ nm}$) oriented parallel to the film surface (see Fig. 2(b)). From 170 °C, in which all molecular interactions were dissociated, slowly melt-crystallized film revealed relatively short nanorods with $L < 1 \mu\text{m}$ and $L_w \sim 30 \text{ nm}$, in comparison to the 130 °C annealed sample (see Fig. 2(c)). As shown in Figures 2(b and c), both the thermal treatments for cast PQT-12 films could considerably improve self-assembled nanostructure and its crystallinity, as early reported.¹² Note that the molten PQT-12 tended to be easily dewetted on the OTS-treated dielectric surface (water contact angle $\sim 105^\circ$). In contrast, cast films exposed by TCB solvent vapor, as plasticizers, revealed nano-aggregates with diameters of 60–80 nm, causing surface undulation in the film (see Fig. 2(d)). It was found that the macroscopic crystal structures of PQT-12 were significantly changed by enhancing the π overlap between the polymer chain backbones. In particular, achieving fine control over the directionality of π -conjugation in PQT-12 domains is currently a key challenge that must be overcome to improve the performance of these devices.

In order to investigate crystalline structures and orientations in the PQT-12 films showing discernible crystal morphologies, synchrotron-based grazing-incidence X-ray diffraction (GIXD) was performed at X9, Brookhaven

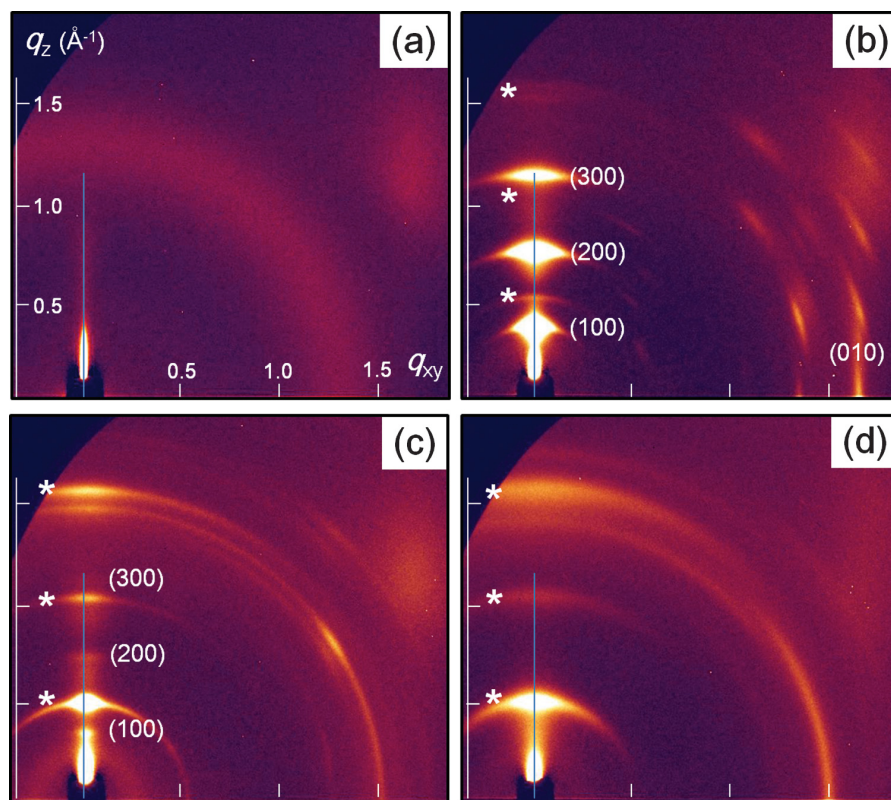


Fig. 3. (a–d) 2D GIXD patterns of PQT-12 thin films on OTS-treated SiO₂ substrates: (a) as-spun; (b) 130 °C annealed; (c) melt-crystallized; (d) solvent-annealed samples, respectively.

National Laboratory: angle of the incident beam was fixed to 0.3° with respect to the OTS-treated SiO_2/Si substrate, because of optimizing X-ray reflections and these resolutions. Figure 3 represents 2D GIXD patterns indicating different crystallinities and chain orientations in these PQT-12 films examined in this paper. It should be noted that because of the geometry of GIXD experiment, the peaks seen along the nominal q_z axis (at $q_{xy} = 0$) do not reflect the true intensity profile in reciprocal space of the corresponding Bragg peaks, due to off-specular diffraction and (at $q_{xy} = 0$).¹⁷ 2D GIXD pattern of the as-spun PQT-12 film only showed intense peak of X-ray reflectivity along the q_z axis and circular hallow ring, suggesting that the chains were oriented parallel to the surface and formed a less-ordered layer formation with a LC structure (see Fig. 3(a)). Due to the preferential chain orientation in as-spun PQT-12 films, annealed samples might have highly crystalline structures via either thermal or solvent annealing. GIXD pattern of the 130 °C annealed sample (Fig. 3(b)) showed strong X-ray reflections of ($h00$) crystal planes and another weak reflections (asterisk-marked peaks, $\sim 1\%$ of (100) peak intensity) along the q_z (out-of-plane) axis, as well as reflection of (010) planes at q_{xy} (in-plane) = 1.65 \AA^{-1} . In this case, the intense peak at $q_z = 0.379 \text{ \AA}^{-1}$ was indicated as the layer spacing, $d_{(100)} = 16.6 \text{ \AA}$, between (100) crystal planes containing π overlapped backbones. In comparison to poly(3-dodecyl thiophene) with $d_{(100)}$ of 25.5 \AA , the considerably small distance between the highly ordered (100) planes supported that side-chains preferred to form an interdigitated structure and were highly tilted with respect to the surface normal. As shown in Figure 3(b), the weak X-ray reflection at $q_z = 0.523 \text{ \AA}^{-1}$ was indicated as a new crystal with much thinner layer spacing, $d_{(100)}$ of ca. 12.0 \AA .

It was found that the polymorphic crystals in PQT-12 films competed together, strongly depending on the post film treatments. In melt-crystallized films, the portion of the thinner crystal phase was significantly increased, when compared to that in the thicker one. In particular, it completely occupied solvent-annealed film, as determined by 2D GIXD patterns showing arc types of crystal reflections (see Figs. 3(c and d)). Figure 4(a) showed out-of-plane X-ray profiles extracted from 2D GIXD patterns of all PQT-12 films examined. Based on AFM and GIXD analyses, the distinguishable crystal phases could be speculated, as shown in Figure 4(b).

The thinner crystal phase was expected as one of PQT-12 polymorphic crystals and had less compact π overlap and coil-like SCs, as determined by $d_{(010)} = 4.16 \text{ \AA}$ and $d_{(100)} \sim 12 \text{ \AA}$, which were much wider π overlap and closer layer spacing distances, respectively, than those (16.8 \AA and 3.80 \AA) of highly ordered crystal structure with interdigitated side-chains.

For cast PQT-12 films, effects of the different π overlap structures and chain orientations on electrical OFET

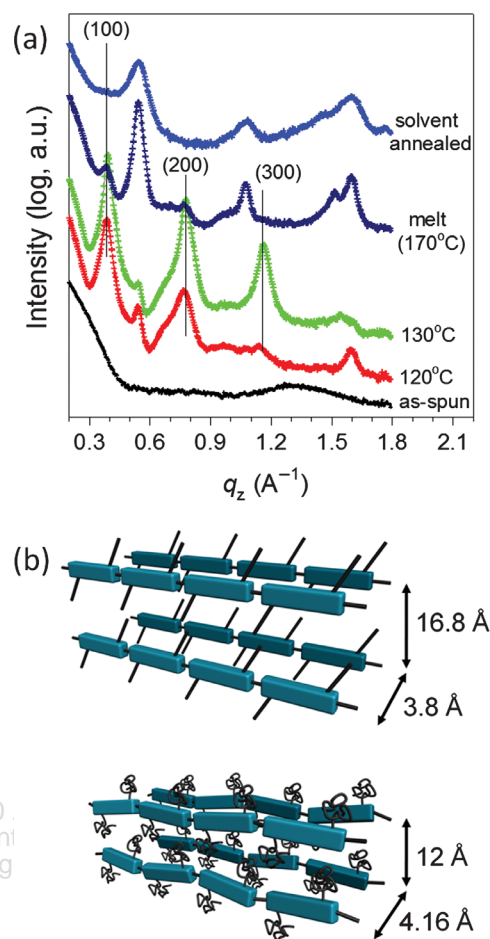


Fig. 4. (a) out-of-plane X-ray profiles extracted from 2D GIXD patterns. (b) Schematic diagrams of chain conformations of PQT-12 in two discernible crystal phases examined.

performances were investigated. In PQT-12 OFETs, bottom Au electrodes were lithographically patterned on the OTS-treated SiO_2/Si substrates by several step procedures illustrated in Figure 5. Then, 50-nm-thick PQT-12 films were spin-cast or further post-treated on the OTS-treated SiO_2/Si substrates including the bottom-contact Au electrodes. Figure 6 represents typical drain current versus drain voltage ($I_D - V_D$) output curves and drain current versus gate voltage ($I_D - V_G$) transfer curves of these OFETs, respectively. In the saturation region, I_D can be described using the following equation,

$$I_D = \frac{WC_i}{2L} \mu_{\text{FET}} (V_G - V_o)^2$$

where μ_{FET} is the field-effect mobility, W is the channel width, L is the channel length, C_i is the capacitance per unit area of the insulation layer ($C_i = 10 \text{ nFcm}^{-2}$).

The 130 °C sample produced the maximum I_D differed by a factor of about 20, when compared to that ($6 \mu\text{A}$)

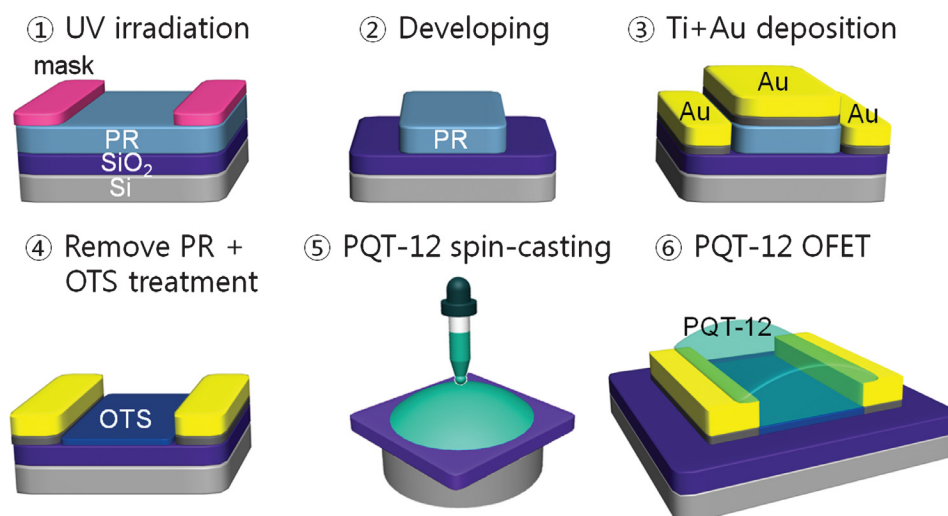


Fig. 5. Device fabrication schemes of bottom-contact Au electrodes and PQT-12 films on OTS-treated SiO₂/Si substrates. (channel length, L and width, W were 10 μm and 1500 μm , respectively.)

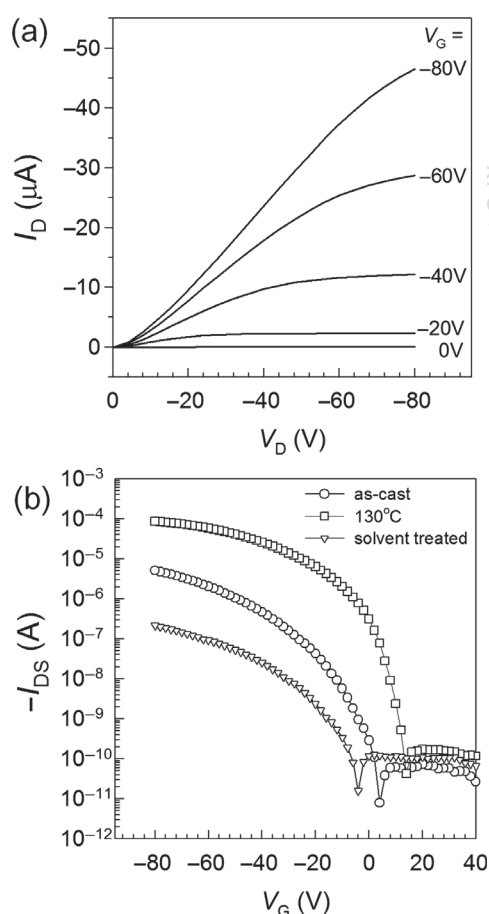


Fig. 6. (a) $I_D - V_D$ output curves of OFET containing 130 $^{\circ}\text{C}$ annealed PQT-12 film. (b) $I_D - V_G$ transfer curves of OFET based on PQT-12 thin films fabricated via different film treatments ($V_D = -80$ V).

of the as-spun sample ($\mu_{\text{FET}} \sim 0.002 \text{ cm}^2\text{V}^{-1}\text{s}^{-1}$) and produced the values of μ_{FET} as high as $0.02 \text{ cm}^2\text{V}^{-1}\text{s}^{-1}$. However, the solvent-annealed sample showing the lowest value of $\mu_{\text{FET}} \sim 6.3 \times 10^{-5} \text{ cm}^2\text{V}^{-1}\text{s}^{-1}$ could be expected, due to small crystal grains and large $d_{(010)}$ of PQT-12, as high potential barriers to transfer charge carriers. For the melt-crystallized samples, however, I_D was not achieved due to dewetted film formation at device channels. In addition, the shift of the threshold voltage in the as-cast and solvent annealed samples to negative V_G is mainly related to the solvent residue or less-ordered π overlap in the PQT-12 films, in comparison to the 130 $^{\circ}\text{C}$ sample (see Fig. 6(b)).

The results strongly supported that one of the key motors to achieve high performance OFETs is the control of π -conjugated structures of organic semiconductors, enhancing charge carrier transports in OFETs. The introduction of hydrophobic self-assembled monolayers (SAMs) and/or ultrathin polymer films on the polar dielectrics has induced well-ordered crystals of π -conjugated organic semiconductors, as well as the minimization of the interfacial charge traps by the surface polar groups. Through chemically anchoring an alkyl silane on an oxide insulator, especially, the SAM-treated dielectrics could provide robust surface hydrophobicity with solution semiconducting layer processes.

3. CONCLUSION

π -conjugated PQT-12 had a liquid crystalline (LC) characteristic, due to enough intervals ($\sim 15.5 \text{ \AA}$) to maximize self-assembly of dodecyl side chains on π -conjugated backbones. However, the relatively lower alkyl content

caused stability issues of PQT-12 solutions during film fabrication with slow solvent evaporation rates, i.e., precipitation or gelation. Here, PQT-12 films were spun-cast on OTS-treated SiO₂/Si substrates from warm trichlorobenzene (80 °C) to introduce smooth film texture. Then, their crystalline structures could be considerably improved via either post heat- or solvent-treatments. At temperatures (125–138 °C) giving a LC state of PQT-12, mobile chains were better migrated into preformed crystals held by intermolecular π – π interaction. Films annealed at 130 °C (for 2 hr) showed highly crystalline nanofibrils, in which dodecyl side-chains were highly interdigitated and narrow intermolecular π overlap distance was 3.80 Å. Via melting or solvent exposure, however, the film crystallized from physically isotropic states at 170 °C or by exposure of TCB vapor grew into less ordered PQT-12 crystals with coil-like conformation of side-chains, resulting in higher π overlap distance of 4.16 Å. The corresponding bottom-contact electrode OFETs were significantly affected by the crystalline structures of PQT-12. As a result, the hole mobilities were the following order: 130 °C annealed > as-spun > TCB-annealed. The usage of LC characteristic allowed us to consistently achieve the desirable crystal structure of PQT-12 and to robustly obtain high field-effect mobility for OFET applications.

Acknowledgment: Financial support was provided by the INHA Research Grant (INHA-40876-01).

References and Notes

1. R. A. Street, W. S. Wong, S. E. Ready, I. L. Chabiny, A. C. Arias, S. Limb, A. Salleo, and R. Lujan, *Mater. Today* 9, 32 (2006).
2. A. N. Sokolov, M. E. Roberts, and Z. Bao, *Mater. Today* 12, 9 (2009).
3. I. McCulloch, M. Heeney, C. Bailey, K. Genevicius, I. MacDonald, M. Shkunov, D. Sparrowe, S. Tierney, R. Wagner, W. Zhang, M. L. Chabiny, R. J. Kline, M. D. McGehee, and M. F. Toney, *Nat. Mater.* 5, 328 (2006).
4. Z. Bao, Y. Feng, A. Dobadalapur, V. R. Raju, and A. J. Lovinger, *Chem. Mater.* 9, 1299 (1997).
5. H. Sirringhaus, T. Kawase, R. H. Friend, T. Shimoda, M. Inbasekaran, W. Wu, and E. P. Woo, *Science* 290, 2123 (2000).
6. Q. Qi, A. Yu, L. Wang, and C. Jiang, *J. Nanosci. Nanotechnol.* 10, 7103 (2010).
7. Y. Yu, *J. Nanosci. Nanotechnol.* 10, 5354 (2010).
8. B. S. Ong, Y. Wu, P. Liu, and S. Gardner, *J. Am. Chem. Soc.* 126, 3378 (2004).
9. H. Yang *Organic Field-Effect Transistors*, edited by Z. Bao and J. Locklin, CRC Press, New York (2007), p. 371.
10. H. E. Katz, Z. Bao, and S. L. Gilat, *Acc. Chem. Res.* 34, 359 (2001).
11. H. Yang, S. W. LeFevre, C. Y. Ryu, and Z. Bao, *Appl. Phys. Lett.* 90, 172116 (2007).
12. N. Zhao, G. A. Botton, S. Zhu, A. Duft, B. S. Ong, Y. Wu, and P. Liu, *Macromolecules* 37, 8307 (2004).
13. Y. Wu, P. Liu, B. S. Ong, T. Srikumar, N. Zhao, G. Botton, and S. Zhu, *Appl. Phys. Lett.* 86, 142102 (2005).
14. B. S. Ong, Y. Wu, P. Liu, and S. Gardner, *Adv. Mater.* 17, 1141 (2005).
15. S. Malik and A. K. Nandi, *J. Phys. Chem B* 108, 597 (2004).
16. W. Y. Huang, P. T. Huang, Y. K. Han, C. C. Lee, T. L. Hsieh, and M. Y. Chang, *Macromolecules* 41, 7485 (2008).
17. H. Yang, S. H. Lim, L. Yang, S. Y. Yang, and C. E. Park, *Adv. Mater.* 19, 2868 (2007).

Received: 26 August 2010. Accepted: 17 December 2010.